Data Oscillation and Convergence of Adaptive FEM

Pedro Morin Ricardo H. Nochetto Kunibert G. Siebert

Abstract

Data oscillation is intrinsic information missed by the averaging process associated with finite element methods (FEM) regardless of quadrature. Ensuring a reduction rate of data oscillation, together with an error reduction based on a posteriori error estimators, we construct a simple and efficient adaptive FEM for elliptic PDE with linear rate of convergence without any preliminary mesh adaptation nor explicit knowledge of constants. Any prescribed error tolerance is thus achieved in a finite number of steps. A number of numerical experiments in 2d and 3d yield quasi-optimal meshes along with a competitive performance.

Key words. A posteriori error estimators, data oscillation, adaptive mesh refinement, convergence, performance, quasi-optimal meshes

1991 AMS subject classification. 65N12, 65N15, 65N30, 65N50, 65Y20

1 Introduction and Main Results

Adaptive procedures for the numerical solution of partial differential equations (PDE) started in the late 70's and are now standard tools in science and engineering. We refer to [13] for references on adaptivity of elliptic PDE, and restrict the list of papers to those strictly related to our work. Adaptive finite element methods (FEM) are indeed a meaningful approach for handling multiscale phenomena and making realistic computations feasible, specially in 3d.

A posteriori error estimators are an essential ingredient of adaptivity. They are computable quantities depending on the computed solution(s) and data that provide information about the quality of approximation and may thus be used to make judicious mesh modifications. The ultimate purpose is to construct a sequence of meshes that would eventually equidistribute the approximation errors, and as a consequence the computational effort. To this end, the a posteriori error estimators are split into element indicators which are then employed to make local mesh modifications by refinement and coarsening. This naturally leads to loops of the form

$$\text{Solve} \;\rightarrow\; \text{Estimate} \;\rightarrow\; \text{Refine / Coarsen.} \tag{1.1}$$

Experience strongly suggests that, starting from a coarse mesh, such an iteration converges within any prescribed error tolerance in a finite number of steps. Except for the rather complete description of the 1d situation by Babuška and Vogelius [2], *convergence* of (1.1) in the multidimensional case is largely an open issue. The fundamental paper [4] of Dörfler for the Poisson equation shows a linear *error reduction* rate for the energy norm towards a preassigned tolerance ϵ in finite steps, provided that

(a) *the initial mesh is sufficiently refined to resolve data within a tolerance* $\mu\epsilon \ll \epsilon$ *(mesh fineness)*;

(b) *the sum of the local error indicators of elements marked for refinement amounts to a fixed portion of the global error estimator (marking strategy).*

We also refer to [5] and [6] for related work. Our results are based on, and in fact improve upon, this idea of Dörfler.

To be more specific, let Ω be a polygonal (polyhedral) and bounded domain of $\mathbb{R}^d$, for $d = 2, 3$, and let u be the solution to the following problem

$$\begin{cases} -\operatorname{div}(A\,\nabla u) = f & \text{in } \Omega, \\ \qquad\qquad\; u = 0 & \text{on } \partial\Omega, \end{cases} \tag{1.2}$$

where $f \in L^2(\Omega)$ and A is a piecewise constant positive definite symmetric matrix. Let $\mathcal{T}_H$ be a conforming triangulation of Ω, with piecewise constant meshsize H, and let u_H denote the piecewise linear finite element solution over $\mathcal{T}_H$ assuming exact integration. This is an ideal situation which helps isolate essential difficulties from quadrature issues; the latter deserve a separate investigation. The following quantity, hereafter called *data oscillation*, will play a fundamental role

$$\operatorname{osc}(f, \mathcal{T}_H) := \left(\sum_{T \in \mathcal{T}_H} \|H(f - f_T)\|_T^2 \right)^{1/2}; \tag{1.3}$$

from now on f_T stands for the mean value of f over T, but may be any piecewise constant approximation to f on T. Such $\operatorname{osc}(f, \mathcal{T}_H)$ measures intrinsic information missing in the averaging process associated with finite elements, which fail to detect fine structures of f. We stress that (1.3) is unrelated to quadrature and quantifies data oscillation with the least amount of information per element, namely one degree of freedom associated to f_T.

In contrast to [4], which imposes the constraint $\left(\sum_{T\in\mathcal{T}_H} \|Hf\|_T^2\right)^{1/2} \le \mu\epsilon$ on the interior residual as a notion of mesh fineness in (a), we claim that $\operatorname{osc}(f, \mathcal{T}_H) \le \mu\epsilon$ is what really matters; this crucial property is derived in §4. We observe that $\operatorname{osc}(f, \mathcal{T}_H)$ is generically of higher order than the interior residual, and so (a) is easier to obtain whereas the original condition of [4] may easily lead to an initial over-refinement (see Example 5.2). As illustrated in Example 3.7, there might be pathological instances when data oscillation and interior residual are comparable and the concept of mesh fineness becomes relevant. To circumvent the restriction of mesh fineness, we propose simple but essential changes to [4] which result in a practical procedure, the *Algorithm C* of §3, whose formulation needs no tolerance ϵ. In addition to marking elements according to (b) in each step, Algorithm C starts from any coarse mesh and ensures one interior node for each marked element together with a linear data oscillation decay. The interior node guarantees suitable error decrease when data oscillation is relatively small. Its need is justified in Examples 3.5 and 3.6, and a proof of the fundamental error reduction property is given in §4. Algorithm C yields the following convergence result, proved in §3.

Main Result: *Let u_k be a sequence of finite element solutions produced by Algorithm C. There exist positive constants C_0 and $\beta < 1$, depending only on given data and the initial grid, such that*

$$|\!|\!| u - u_k |\!|\!|_\Omega \leq C_0\, \beta^k, \tag{1.4}$$

where the energy norm is given by $|\!|\!| v |\!|\!|_\Omega = (\int_\Omega \nabla v \cdot A \nabla v)^{1/2}$. The initial coarse mesh need not be adjusted to resolve data to any tolerance, and no explicit constants are needed for Algorithm C to work.

A few comments and comparisons are now in order.

- Any prescribed error tolerance ϵ may be met in finite steps, as in [4], but without any special tuning of the initial mesh in terms of ϵ; this issue is important and its practical implications are fully examined in Example 5.2 of §5.
- Depending on the flatness of u, the meshsize H may not necessarily tend to zero, which makes this a nonstandard finite element asymptotic statement.
- Even though no stability constants are required for Algorithm C, nor for convergence, the constant in the upper bound of the residual-type a posteriori error estimate is needed to stop the iterations; this is customary in adaptivity [13].
- Inequality (1.4) does not imply that the error decays in every single step as in [4], and Example 3.7 shows that it may be constant for a number of steps due to unresolved data oscillation.
- The interior node created by Algorithm C guarantees suitable error decrease when data oscillation is small, and is discussed in Examples 3.5 and 3.6. This theoretical requirement may be viewed as a looking-ahead strategy, and the 2d and 3d experiments of §5 clearly indicate no additional computational expense.

In §5 we present several illuminating numerical experiments computed within the finite element toolbox ALBERT [11, 12]. The first example is the crack problem, which exhibits a point singularity of the form $r^{1/2}$. The second example corresponds to intersecting interfaces (discontinuous coefficients) and a much more severe singularity of the form r^γ with γ arbitrarily close to 0. In both cases f is constant and thus $\operatorname{osc}(f, \mathcal{T}_H) = 0$. We finally discuss a 2d and 3d example with variable f and thereby test the effect of data oscillation. It turns out that such an effect is negligible for smooth f (relative to the underlying mesh). This provides a heuristic explanation for the success of most adaptive strategies which disregard the issue of data oscillation altogether. The experiments reveal also that the resulting meshes are quasi-optimal: the error decays proportionally to $N^{-1/d}$, N being the number of degrees of freedom. Our theory, however, does not explain this important property. Mesh optimality has been recently studied in [3] via wavelet algorithms which resort to the entire wavelet expansions of u and f. These full expansions are not available in practice though, and somehow encode the missing information of data oscillation.

This paper is organized as follows. In §2 we recall the standard a posteriori residual-type error estimators which constitute the core of adaptivity [13]. In §3 we present Algorithm C, justify its various steps, and prove the Main Result. In §4 we derive the crucial error reduction property, thereby closing the gap. We conclude with several 2d and 3d experiments in §5 which fully document the competitive performance of our novel adaptive strategy.

2 A Posteriori Error Estimators

We start this section with some useful notation. For an open set $G \subset \mathbb{R}^d$ we denote by $H^1(G)$ the usual Sobolev space of functions in $L^2(G)$ whose first derivatives are also in $L^2(G)$, endowed with the norm

$$\|u\|_{H^1(\Omega)} := \left(\|u\|_G^2 + \|\nabla u\|_G^2\right)^{1/2}$$

where $\|\cdot\|_G$ stands for the $L^2(G)$-norm.

Since A is piecewise constant, symmetric and positive definite, the bilinear form $((\cdot\,,\,\cdot))_G$ defined for any open set $G \subset \Omega$ by

$$((u\,,\,v))_G := \int_G A\nabla u \cdot \nabla v,$$

is bounded, and $((\cdot\,,\,\cdot))_\Omega$ is coercive on $H_0^1(\Omega)$, i.e., there exist constants $0 < c_a \le C_a < \infty$ such that

$$((v\,,\,w))_G \le C_a \|v\|_{H^1(G)} \|w\|_{H^1(G)}, \qquad \forall\, v, w \in H^1(G), \tag{2.1}$$

$$c_a \|v\|_{H^1(\Omega)}^2 \le ((v\,,\,v))_\Omega, \qquad \forall\, v \in H_0^1(\Omega). \tag{2.2}$$

This implies, in particular, that the seminorm $|\!|\!|\cdot|\!|\!|_G$ defined by $|\!|\!|v|\!|\!|_G^2 := ((v\,,\,v))_G$ is equivalent to the $H_0^1(\Omega)$-norm when $G = \Omega$.

In view of (2.1) and (2.2), problem (1.2) admits a unique weak solution u for any $f \in L^2(\Omega)$, i.e.,

$$u \in H_0^1(\Omega): \qquad ((u\,,\,v))_\Omega = \int_\Omega fv, \qquad \forall\, v \in H_0^1(\Omega). \tag{2.3}$$

Let $\mathcal{T}_H$ be a conforming regular triangulation of Ω, with piecewise constant meshsize H, i.e., $H|_T = \mathrm{diam}(T)$. Let $\mathbb{V}^H$ be the space of continuous piecewise linear functions over $\mathcal{T}_H$, and let $\mathbb{V}_0^H$ be the subspace of functions of $\mathbb{V}^H$ that vanish at the boundary. Let u_H denote the solution of the discrete problem

$$u_H \in \mathbb{V}_0^H : \qquad ((u_H\,,\,\phi))_\Omega = \int_\Omega f\phi, \quad \forall\, \phi \in \mathbb{V}_0^H. \tag{2.4}$$

The function f_H will denote the piecewise constant function over $\mathcal{T}_H$ that, restricted to each element $T \in \mathcal{T}_H$, is equal to the mean value f_T of f on T.

We denote by $\mathcal{S}_H$ the set of sides of the triangulation $\mathcal{T}_H$ that do not belong to the boundary $\partial\Omega$ of the domain Ω. For $S \in \mathcal{S}_H$, the domain Ω_S is the union of the two elements in $\mathcal{T}_H$ sharing S, and H_S denotes the diameter of S. We assume that all partitions $\mathcal{T}_H$ match the discontinuities of A, i.e., the jumps of A are located on inter-element boundaries $S \in \mathcal{S}_H$.

We now recall the *residual-type* a posteriori error estimators for (2.3) and (2.4) [1], [13]. Subtracting (2.4) from (2.3) and integrating by parts yields the following well-known relation between the error $u - u_H$ and the residuals

$$((u - u_H\,,\,\phi)) = \sum_{T\in\mathcal{T}_H} \int_T f(\phi - \mathcal{I}_H\phi) + \sum_{S\in\mathcal{S}_H} \int_S J_S(\phi - \mathcal{I}_H\phi), \tag{2.5}$$

for all $\phi \in H_0^1(\Omega)$. Hereafter, $\mathcal{I}_H$ denotes the Clément interpolation operator, and $J_S = [A\nabla u_H]_S \cdot \nu$ represents the jump of flux across side S which is independent of the orientation of the unit normal ν. Let η_S be the (local) error indicator associated with side $S \in \mathcal{S}_H$

$$\eta_S^2 := \left\| H_S^{\frac{1}{2}} J_S \right\|_S^2 + \|H\,f\|_{\Omega_S}^2\,, \tag{2.6}$$

which consists of the jump and interior residuals, respectively. Let η_H be the (global) error estimator given by

$$\eta_H^2 := \sum_{S\in\mathcal{S}_H} \eta_S^2.$$

Upon taking $\phi = u - u_H$ in (2.5), and using interpolation theory, the following result emerges [1], [13].

Lemma 2.1 (Upper Bound). *There exists a constant C_1, depending only on the minimum angle of $\mathcal{T}_H$, C_a and c_a, such that*

$$|\!|\!| u - u_H |\!|\!|_\Omega^2 \le C_1 \eta_H^2. \tag{2.7}$$

An early indication of the crucial role of oscillation is given by the (local) lower bound [1], [13]. The construction by Verfürth [13] will be important later.

Lemma 2.2 (Lower Bound). *There exist constants C_2, C_3, depending only on the minimum angle of $\mathcal{T}_H$, C_a and c_a, such that*

$$C_2\eta_S^2 - C_3\|H(f - f_H)\|_{\Omega_S}^2 \le |\!|\!| u - u_H |\!|\!|_{\Omega_S}^2\,. \tag{2.8}$$

Remark 2.3. Suppose that $\|H(f - f_H)\|_{\Omega_S}$ is small with respect to η_S. In such a case, the significance of (2.8) is that the size of η_S provides reliable information about the size of $\|u - u_H\|_{\Omega_S}$. This explains why refining elements with large error indicators usually tends to equidistribute approximation errors, an ultimate goal of adaptivity.

Remark 2.4. It is worth realizing that f_H in (2.8) could be any piecewise polynomial and not just the mean value of f over the elements. This additional freedom in measuring data oscillation disappears in dealing with consecutive discrete functions u_H and u_h. This issue will be central to our discussions of §4.

3 Algorithm C and Convergence

We start with a marking strategy for *error reduction* due to Dörfler [4]:

Marking Strategy E

Given a parameter $0 < \theta < 1$:

1. Select in $\hat{\mathcal{S}}_H$ some sides such that
$$\left(\sum_{S \in \hat{\mathcal{S}}_H} \eta_S^2 \right)^{1/2} \geq \theta \eta_H .$$
2. Let $\hat{\mathcal{T}}_H$ be the set of elements with one side in $\hat{\mathcal{S}}_H$ and mark all these elements.

This marking strategy ensures that we choose sufficiently many sides S such that their contributions η_S constitute a fixed proportion of the global error estimator η_H. Using the Marking Strategy E, we have the following error reduction result which is proved in §4.

Theorem 3.1 (Error Reduction). *Let $\mathcal{T}_H$ be a triangulation of Ω, and let $\mathcal{T}_h$ be a triangulation obtained from $\mathcal{T}_H$ by refining at least every element marked according to Strategy E in such a way that a node is created in the element interior. There exist constants $\mu > 0$ and $0 < \alpha < 1$, depending only on the minimum angle, θ, C_a and c_a, such that for any $\epsilon > 0$, if*

$$\operatorname{osc}(f, \mathcal{T}_H) \leq \mu \epsilon, \tag{3.1}$$

then either $\|u - u_H\|_\Omega \leq \epsilon$ or the solution u_h on the mesh $\mathcal{T}_h$ satisfies

$$\|u - u_h\|_\Omega \leq \alpha \, \|u - u_H\|_\Omega .$$

Remark 3.2. This result establishes an error reduction provided the current error is larger than the desired tolerance ϵ. In [4], Dörfler proves a similar result assuming that $\left(\sum_{T\in\mathcal{T}_H}\|Hf\|_T^2\right)^{1/2}\le\mu\epsilon$ instead of (3.1). The notion of *mesh fineness* given by (3.1) is generically of higher order than the one given in [4].

Remark 3.3. The requirement of having a node of the refined grid $\mathcal{T}_h$ *inside* each marked element of $\mathcal{T}_H$ is an essential difference with [4]. This requirement is responsible for the new measure of data approximation. Its implementation in 2d and 3d by bisection is discussed in §5.

Remark 3.4. A repeated application of the Marking Strategy E, and the special refinement of Theorem 3.1, leads to an iterative process that converges in a finite number of steps to a discrete solution within tolerance ϵ; this is the main contribution of [4]. However, if this process were to be restarted with a stringent tolerance, data oscillation might not satisfy (3.1). Consequently, this strategy alone does *not* yield an asymptotically convergent algorithm.

To shed light on the ingredients for convergence, we discuss three examples. They show the importance of the special refinement of Theorem 3.1 with an interior node to obtain an error reduction, as well as the necessity of controlling data oscillation.

Example 3.5 (Interior Node 1). This example shows the necessity of creating an interior node inside each refined triangle. Consider Problem (1.2) with $A = Id$, $f\equiv 1$ and $\Omega=(0,1)\times(0,1)$. Let $\mathcal{T}_H$ be the grid with nodes $\{(0,0),(1,0),(1,1),(0,1),(\frac12,\frac12)\}$ (see Figure 1).

Now, let us call ϕ_1 the nodal basis function of $\mathbb{V}^H$ that corresponds to the node $(\frac12,\frac12)$. Then, the finite element solution u_H on this grid is $c_1\phi_1$, where

$$c_1\int_\Omega \nabla\phi_1\cdot\nabla\phi_1=\int_\Omega f\phi_1 \qquad\Rightarrow\qquad c_1=\frac{1/3}{4}=\frac{1}{12}.$$

Let $\mathcal{T}_h$ be the grid obtained from $\mathcal{T}_H$ by performing two bisections on each triangle of $\mathcal{T}_H$ using the newest-vertex bisection and assuming that $(\frac12,\frac12)$ is the newest vertex on the initial grid. This is the standard refinement performed in [4], and does not lead to an interior node in the refined elements (see Figure 1). Then, we get a larger set of nodes, which we enumerate as in Figure 1. Let us call φ_i the nodal basis function of $\mathbb{V}^h$ that corresponds to the node i of $\mathcal{T}_h$, $i=1,2,\ldots,5$. The finite element solution u_h on this refined grid is

$$u_h=\sum_{i=1}^5 c_i\varphi_i$$

where $c:=(c_i)_{i=1}^5$ satisfies the equation $Kc=b$, with K and b given by

$$K_{ij}=\int_\Omega\nabla\varphi_i\nabla\varphi_j,\quad i,j=1,2,\ldots,5,$$

$$b_i=\int_\Omega f\nabla\varphi_i,\quad i=1,2,\ldots,5.$$

We easily see that

$$K = \begin{bmatrix} 4 & 0 & -1 & 0 & 0 \\ 0 & 4 & -1 & 0 & 0 \\ -1 & -1 & 4 & -1 & -1 \\ 0 & 0 & -1 & 4 & 0 \\ 0 & 0 & -1 & 0 & 4 \end{bmatrix} \quad \text{and} \quad b = \begin{bmatrix} 1/12 \\ 1/12 \\ 1/6 \\ 1/12 \\ 1/12 \end{bmatrix}$$

which gives $c = (\frac{1}{24}, \frac{1}{24}, \frac{1}{12}, \frac{1}{24}, \frac{1}{24})^t$, and consequently, $u_h = u_H$. This equality implies that the errors corresponding to both grids $\mathcal{T}_H$ and $\mathcal{T}_h$ are equal. We conclude that without one interior node in at least one triangle, no error reduction is obtained even when $\operatorname{osc}(f, \mathcal{T}_H) = 0$ and $|||u - u_H|||_\Omega > 0$.

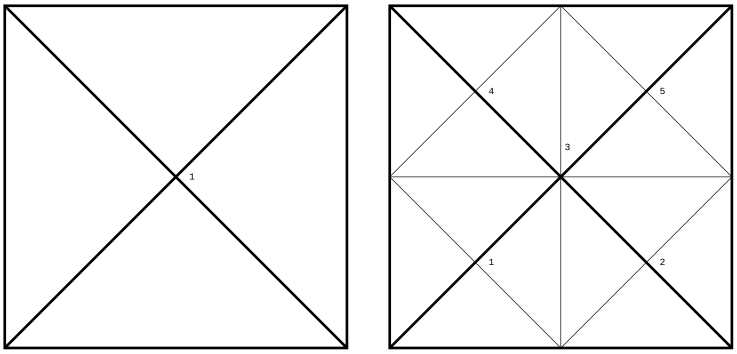

Figure 1: Refinement by bisecting all triangles twice.

Example 3.6 (Interior Node 2). At a first sight, it may seem that the situation of Example 3.5 may occur only at the first refinement step. This example shows that such a situation can also happen at any refinement step n.

Fix $n \in \mathbb{N}$ and consider (1.2) with $A = Id$, $\Omega = (0,1)^2$ and f given by

$$f(x) = \begin{cases} 1 & \text{if } x \in (i\,2^{-n}, (i+1)\,2^{-n}) \times (j\,2^{-n}, (j+1)\,2^{-n}) \text{ and } i+j \text{ odd} \\ -1 & \text{otherwise;} \end{cases}$$

see Figure 2. Then, if we start with $\mathcal{T}_0$ equal to the grid $\mathcal{T}_H$ of Example 3.5, and ϕ_1 also as in Example 3.5, we have that ϕ_1 is orthogonal to f and consequently $u_0 \equiv 0$. If we now define recursively $\mathcal{T}_{k+1}$, $k = 0, 1, \dots$ as the grid that results from $\mathcal{T}_k$ by performing two newest-vertex bisections on every triangle (see Figure 2), we will have $u_k \equiv 0$ for $k = 0, 1, \dots, n-1$, due to the fact that f is orthogonal to the basis functions of $\mathcal{T}_k$ for $k = 0, 1, \dots, n-1$.

For $k = n$ the solution u_n will not be zero anymore, but it will be zero along the lines where f changes sign due to the symmetry of the problem, and the same will happen with u_{n+1}. Then, if we observe u_n and u_{n+1} in a fixed square where f is constant, they behave exactly as u_H and u_h do in Example 3.5, and

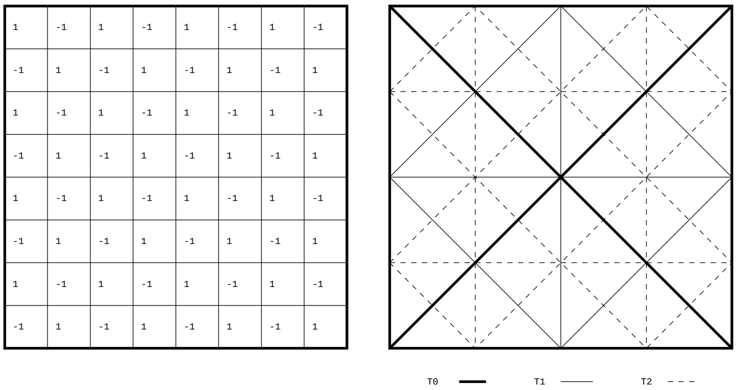

Figure 2: Values of the function f of Example 3.6 for $n = 3$ (left), and grids $\mathcal{T}_k$ for $k = 0, 1, 2$ (right).

consequently $u_n = u_{n+1}$, which means that the error is not decreased, even when the oscillation $\operatorname{osc}(f, \mathcal{T}_n)$ is zero.

Example 3.7 (Data Oscillation). This example shows that if the data oscillation $\operatorname{osc}(f, \mathcal{T}_H)$ is not small, then, even introducing an interior node on all elements, the error may not decrease. To see this, consider the Example 3.6

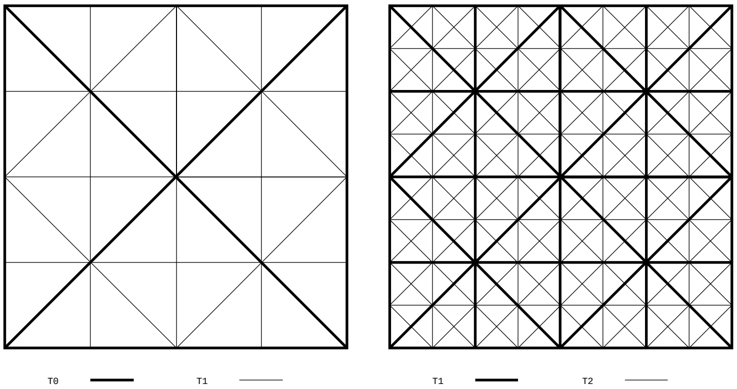

Figure 3: Resulting grid $\mathcal{T}_1$ (left) and $\mathcal{T}_2$ (right) after performing three bisections on each element of $\mathcal{T}_0$ and $\mathcal{T}_1$, respectively.

for some fixed large $n \in \mathbb{N}$. Observe now that if we obtain $\mathcal{T}_{k+1}$ by performing *three* bisections on all the elements of $\mathcal{T}_k$, then three new nodes are created on the edge opposite to the newest vertex in addition to an interior node per element (see Figure 3). Even though this refinement is stronger than required by Theorem 3.1 in each step, the solutions u_k will all be zero for $k < 2n/3$.

We conclude from Examples 3.5 and 3.6 that the interior node is necessary to obtain an error decrease, and from Example 3.7 that this may not be sufficient if the mesh does not resolve the oscillation of data. Therefore, in order to obtain an *asymptotically convergent* sequence of discrete solutions we must readjust the mesh to resolve $\operatorname{osc}(f, \mathcal{T}_H)$ according to a decreasing tolerance. The following simple results guarantee that this is always possible. The first lemma considers the worst scenario situation of f just in $L^2(\Omega)$, whereas the second lemma addresses the case of f piecewise smooth.

Lemma 3.8. *Let $0 < \gamma < 1$ be the reduction factor of element size associated with one refinement step. Given $0 < \hat{\theta} < 1$, let $\hat{\alpha} := (1 - (1-\gamma^2)\hat{\theta}^2)^{1/2}$. Let $\hat{\mathcal{T}}_H$ be a subset of $\mathcal{T}_H$ such that*

$$\operatorname{osc}(f, \hat{\mathcal{T}}_H) \geq \hat{\theta} \operatorname{osc}(f, \mathcal{T}_H). \tag{3.2}$$

If $\mathcal{T}_h$ is a triangulation obtained from $\mathcal{T}_H$ by refining at least every element in $\hat{\mathcal{T}}_H$, then the following data oscillation reduction occurs

$$\operatorname{osc}(f, \mathcal{T}_h) \leq \hat{\alpha} \operatorname{osc}(f, \mathcal{T}_H). \tag{3.3}$$

Proof. Let $T \in \mathcal{T}_h$ be an element contained in $\hat{T} \in \mathcal{T}_H$. Since $f_T = |T|^{-1} \int_T f$ is the L^2-projection of f onto the space of piecewise constants over T, we have

$$\|f - f_T\|_T \leq \|f - f_{\hat{T}}\|_T.$$

Since $h_T \leq \gamma h_{\hat{T}}$, we discover that

$$\begin{aligned}
\operatorname{osc}(f, \mathcal{T}_h)^2 &= \sum_{T \in \mathcal{T}_h} h_T^2 \|f - f_T\|_T^2 \\
&\leq \gamma^2 \sum_{\hat{T} \in \hat{\mathcal{T}}_H} h_{\hat{T}}^2 \|f - f_{\hat{T}}\|_{\hat{T}}^2 + \sum_{T \in \mathcal{T}_H \setminus \hat{\mathcal{T}}_H} h_T^2 \|f - f_T\|_T^2 \\
&= (\gamma^2 - 1) \operatorname{osc}(f, \hat{\mathcal{T}}_H)^2 + \operatorname{osc}(f, \mathcal{T}_H)^2 \leq \hat{\alpha}^2 \operatorname{osc}(f, \mathcal{T}_H)^2. \qquad \square
\end{aligned}$$

Lemma 3.9. *Let f be piecewise H^s for $0 < s \leq 1$ over the initial mesh, where H^s stands for the space of functions f with fractional derivative $D^s f$ of order s in L^2. Let data oscillation be redefined by*

$$\operatorname{osc}(f, \mathcal{T}_h) := \left(\sum_{T \in \mathcal{T}_h} h_T^{2+2s} \|D^s f\|_T^2 \right)^{1/2}.$$

Let $\hat{\alpha} := (1 - (1 - \gamma^{2+2s})\hat{\theta}^2)^{1/2}$, where γ and $\hat{\theta}$ are defined in Lemma 3.8. If $\mathcal{T}_h$ is as in Lemma 3.8, then

$$\operatorname{osc}(f, \mathcal{T}_h) \leq \hat{\alpha} \operatorname{osc}(f, \mathcal{T}_H). \tag{3.4}$$

Proof. It suffices to use that $h_T \leq \gamma h_{\hat{T}}$ for all $T \in \mathcal{T}_h$ contained in $\hat{T} \in \mathcal{T}_H$, and argue as in Lemma 3.8. $\square$

We point out that γ depends only on the minimal angle of the initial mesh, and that $\gamma \leq 1/2$ in 2d provided one interior node is created per marked element; we refer to Figure 5 of §5. This implies that the reduction rate squared of Lemma 3.9 is $\hat{\alpha}^2 \leq 1 - 15\hat{\theta}^2/16 \approx 1 - \hat{\theta}^2$ in 2d provided f is piecewise H^1.

Taking into account that a subset $\hat{\mathcal{T}}_H$ of $\mathcal{T}_H$ is already selected by Marking Strategy E, the following procedure, in conjunction with Lemmas 3.8 or 3.9, guarantees a *data oscillation* decrease by a factor $\hat{\alpha} < 1$.

Marking Strategy D

Given a parameter $0 < \hat{\theta} < 1$ and the subset $\hat{\mathcal{T}}_H \subset \mathcal{T}_H$ produced by Marking Strategy E:

1. Enlarge $\hat{\mathcal{T}}_H$ such that

$$\operatorname{osc}(f, \hat{\mathcal{T}}_H) \geq \hat{\theta} \operatorname{osc}(f, \mathcal{T}_H).$$

2. Mark all elements in $\hat{\mathcal{T}}_H$ for refinement.

In light of Theorem 3.1, Examples 3.5, 3.6 and 3.7, and Lemmas 3.8 and 3.9, we are now in the position to formulate the Algorithm C and prove its asymptotic convergence.

Convergent Algorithm C

Choose parameters $0 < \theta, \hat{\theta} < 1$.

1. Pick up any initial mesh $\mathcal{T}_0$ such that A is piecewise constant over $\mathcal{T}_0$.
2. Solve the system on $\mathcal{T}_0$ for the discrete solution u_0.
3. Let $k = 0$.
4. Compute the local indicators η_S.
5. Construct $\hat{\mathcal{T}}_k \subset \mathcal{T}_k$ by Marking Strategy E and parameter θ.
6. Enlarge $\hat{\mathcal{T}}_k$ by Marking Strategy D and parameter $\hat{\theta}$.
7. Refine every element in $\hat{\mathcal{T}}_k$ in such a way that a node is created in the element interior; let $\mathcal{T}_{k+1}$ be the new mesh.
8. Solve the system on $\mathcal{T}_{k+1}$ for the discrete solution u_{k+1}.
9. Let $k = k + 1$ and go to Step 4.

Theorem 3.10 (Convergence). *For $0 < \theta, \hat{\theta} < 1$, let $0 < \alpha < 1$, $\mu > 0$ be given by Theorem 3.1 and $0 < \hat{\alpha} < 1$ by Lemmas 3.8 or 3.9. Let*

$$\beta := \max(\alpha, \hat{\alpha}), \qquad C_0 := \max\Big(|\!|\!| u - u_0 |\!|\!|_\Omega \,, \frac{\operatorname{osc}(f, \mathcal{T}_0)}{\alpha\mu} \Big). \tag{3.5}$$

Algorithm C *produces a convergent sequence $\{u_k\}_{k\in\mathbb{N}_0}$ of discrete solutions satisfying for all $k \geq 0$*

$$|\!|\!| u - u_k |\!|\!|_\Omega \leq C_0 \, \beta^k. \tag{3.6}$$

Proof. We argue by induction. Such a bound holds trivially for $k = 0$. We assume that (3.6) holds for k. Then, we have either

$$\text{(i)} \quad |\!|\!| u - u_k |\!|\!|_\Omega > C_0 \, \beta^{k+1}, \qquad \text{or} \qquad \text{(ii)} \quad |\!|\!| u - u_k |\!|\!|_\Omega \leq C_0 \, \beta^{k+1}.$$

In case (i), we see from Step 6 of Algorithm C that $\operatorname{osc}(f, \mathcal{T}_k) \leq \hat{\alpha}^k \operatorname{osc}(f, \mathcal{T}_0) \leq \beta^k \operatorname{osc}(f, \mathcal{T}_0)$ and, consequently, that for $\epsilon := C_0 \, \beta^{k+1}$

$$\operatorname{osc}(f, \mathcal{T}_k) \leq \mu C_0 \alpha \beta^k \leq \mu C_0 \beta^{k+1} = \mu\epsilon.$$

Since $|\!|\!| u - u_k |\!|\!|_\Omega > \epsilon$, we may then combine Theorem 3.1 with (3.6) to arrive at

$$|\!|\!| u - u_{k+1} |\!|\!|_\Omega \leq \beta \, |\!|\!| u - u_k |\!|\!|_\Omega \leq C_0 \, \beta^{k+1}.$$

On the other hand, exploiting that $\mathcal{T}_{k+1}$ is a refinement of $\mathcal{T}_k$, and thus the error must not increase, we can handle case (ii) as follows:

$$|\!|\!| u - u_{k+1} |\!|\!|_\Omega \leq |\!|\!| u - u_k |\!|\!|_\Omega \leq C_0 \, \beta^{k+1}.$$

This completes the induction procedure and the proof. □

Remark 3.11. Algorithm C is fully practical in that it only needs parameters θ, $\hat{\theta}$. The unknown constants α, $\hat{\alpha}$ and μ are not explicitly needed by Algorithm C, but they dictate the convergence rate.

Remark 3.12. Stopping the sequence $\{u_k\}$ to achieve an error tolerance is the only instance that requires the constant C_1 of Lemma 2.1. This difficulty, associated with residual-type estimators, is customary in the literature though.

Remark 3.13. In view of Lemma 3.9 we expect data oscillation to yield rather minor additional refinement to Step 5. This is confirmed by the numerical experiments of Example 5.4 in both 2d and 3d, and provides some solid theoretical grounds for the convergence of adaptive strategies which disregard data oscillation altogether.

4 Error Reduction

In this section we prove Theorem 3.1. The following orthogonality result is essential and gives us an idea of how to proceed.

Lemma 4.1. *If $\mathcal{T}_h$ is a local refinement of $\mathcal{T}_H$, such that $\mathbb{V}^H \subset \mathbb{V}^h$, the following relation holds*

$$|\!|\!| u - u_h |\!|\!|_\Omega^2 = |\!|\!| u - u_H |\!|\!|_\Omega^2 - |\!|\!| u_H - u_h |\!|\!|_\Omega^2 . \tag{4.1}$$

Proof. By Galerkin orthogonality, $((u - u_h \,,\, v))_\Omega = 0$ for all $v \in \mathbb{V}^h$, whence $u_h - u_H \in \mathbb{V}^h$ is perpendicular to $u - u_h$. Therefore, since $u - u_H = (u - u_h) + (u_h - u_H)$, the assertion (4.1) follows from the Pythagoras Theorem. □

We can see from this lemma that the error reduction is exactly $|\!|\!| u_H - u_h |\!|\!|_\Omega^2$. In order to guarantee that the error decreases a fixed proportion of the current error, we have to bound $|\!|\!| u_H - u_h |\!|\!|_\Omega^2$ from below by $|\!|\!| u - u_H |\!|\!|_\Omega^2$. In view of Lemma 2.2, this reduces to show a lower bound in terms of η_H^2. The following lemma establishes a *local* lower bound for the error decrease in terms of the *local error indicators.* This result will be needed, in conjunction with Lemma 2.1, to prove a *global lower bound* of the error decrease in terms of the current error.

Lemma 4.2. *Let $\mathcal{T}_h$ be a triangulation obtained from $\mathcal{T}_H$ by refining at least every element marked according to Strategy E in such a way that a node is created in the element interior. Then, there exist constants $C_4, C_5 \ge 1$, depending only on the minimum angle and on c_a, C_a, such that, for all $S \in \hat{\mathcal{S}}_H$ we have*

$$\eta_S^2 \le C_4 \, |\!|\!| u_h - u_H |\!|\!|_{\Omega_S}^2 + C_5 \big\| H(f - f_H) \big\|_{\Omega_S}^2 . \tag{4.2}$$

Before getting into the proof of this lemma, observe that this result is similar to the result of Lemma 2.2. Their main differences are that here we get a lower bound for $|\!|\!| u_h - u_H |\!|\!|_{\Omega_S}$ instead of $|\!|\!| u - u_H |\!|\!|_{\Omega_S}$, and that f_H stands for a piecewise *constant* approximation of f, i.e., f_H has only one degree of freedom in each triangle $T \in \mathcal{T}_H$.

Proof of Lemma 4.2. We split the proof into several steps.
1. We claim that there exists an auxiliary function $\phi \in \mathbb{V}^h$, satisfying $\phi|_{\partial\Omega_S} = 0$ together with the two conditions

$$\int_{\Omega_S} f_H \phi + \int_S J_S \phi = \big\| H f_H \big\|_{\Omega_S}^2 + \big\| H_S^{\frac{1}{2}} J_S \big\|_S^2, \tag{4.3}$$

$$\|\nabla\phi\|_{\Omega_S}^2 \le C \left(\|H f_H\|_{\Omega_S}^2 + \big\| H_S^{\frac{1}{2}} J_S \big\|_S^2 \right), \tag{4.4}$$

where the constant C depends only on the minimum angle. We postpone the construction of ϕ and show first how to exploit it.
2. Since $\phi \in \mathbb{V}^h$ and vanishes on $\partial\Omega_S$, integration by parts yields

$$\begin{aligned} ((u_h - u_H \,,\, \phi))_{\Omega_S} &= \int_{\Omega_S} f\phi + \int_S J_S \phi \\ &= \int_{\Omega_S} f_H \phi + \int_S J_S \phi + \int_{\Omega_S} (f - f_H)\phi. \end{aligned}$$

Using (2.1) and (4.3), the Poincaré inequality $\|\phi\|_{\Omega_S} \leq CH_S\|\nabla\phi\|_{\Omega_S}$, we obtain

$$\begin{aligned}\|Hf_H\|_{\Omega_S}^2 + \|H_S^{\frac{1}{2}}J_S\|_S^2 &= ((u_h - u_H\,,\,\phi))_{\Omega_S} - \int_{\Omega_S}(f - f_H)\phi \\ &\leq \|\!|u_h - u_H|\!\|_{\Omega_S}\,\|\!|\phi|\!\|_{\Omega_S} + \|f - f_H\|_{\Omega_S}\|\phi\|_{\Omega_S} \\ &\leq C\left(\|\!|u_h - u_H|\!\|_{\Omega_S} + \|H(f - f_H)\|_{\Omega_S}\right)\|\nabla\phi\|_{\Omega_S}.\end{aligned}$$

In view of (4.4) we thus obtain

$$\|Hf_H\|_{\Omega_S}^2 + \left\|H_S^{\frac{1}{2}}J_S\right\|_S^2 \leq C\,\|\!|u_h - u_H|\!\|_{\Omega_S}^2 + C\,\|H(f - f_T)\|_{\Omega_S}^2\,.$$

3. By virtue of this and the triangle inequality, we get

$$\begin{aligned}\eta_S^2 &= \left\|H_S^{\frac{1}{2}}J_S\right\|_S^2 + \|H\,f\|_{\Omega_S}^2 \\ &\leq 2\left(\left\|H_S^{\frac{1}{2}}J_S\right\|_S^2 + \|H\,f_T\|_{\Omega_S}^2 + \|H\,(f - f_T)\|_{\Omega_S}^2\right) \\ &\leq C_4\,\|\!|u_h - u_H|\!\|_{\Omega_S}^2 + C_5\,\|H(f - f_T)\|_{\Omega_S}^2\,,\end{aligned}$$

which proves the assertion (4.2).

4. To complete the proof it remains to construct ϕ. To do so, let us define φ_S, φ_1, and φ_2 to be the nodal basis functions of $\mathbb{V}^h$ which are equal to one at the midpoint x_S of S, and at the interior nodes x_1, x_2 of T_1 and T_2 respectively; here T_1 and T_2 denote the two elements of $\mathcal{T}_H$ sharing S (see Figure 4). Next,

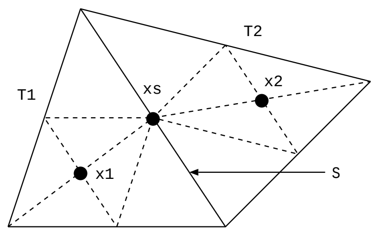

Figure 4: Example of a refined two-element patch $\Omega_S = T_1 \cup T_2$ in 2d.

consider $\phi = \alpha_S\varphi_S + \beta_1\varphi_1 + \beta_2\varphi_2$, where the constants α_S, β_1 and β_2 will be determined later. If $f_i := f_{T_i}$ and $H_i := H_{T_i}$, we can write

$$\int_{\Omega_S} f_H\phi + \int_S J_S\phi = \alpha_S\int_S J_S\varphi_S + \sum_{i=1,2}\Big(\beta_i\int_{T_i} f_i\varphi_i + \alpha_S\int_{T_i} f_i\varphi_S\Big), \qquad (4.5)$$

because the supports of φ_1 and φ_2 do not overlap. Since choosing

$$\alpha_S = \begin{cases} \dfrac{\left\|H_S^{\frac{1}{2}}J_S\right\|_S^2}{\int_S J_S\varphi_S} & \text{if } J_S \neq 0, \\ 0 & \text{otherwise,}\end{cases}$$

and for $i = 1, 2$

$$\beta_i = \begin{cases} \dfrac{\|H_i f_i\|_{T_i}^2 - \alpha_S \int_{T_i} f_i \varphi_S}{\int_{T_i} f_i \varphi_i} & \text{if } f_i \neq 0, \\ 0 & \text{otherwise,} \end{cases}$$

the condition (4.3) is satisfied, it only remains to prove (4.4). To this end, we observe first that

$$\|\nabla \phi\|_{\Omega_S} \leq |\alpha_S| \, \|\nabla \varphi_S\|_{\Omega_S} + \sum_{i=1,2} |\beta_i| \, \|\nabla \varphi_i\|_{\Omega_S} \,,$$

and estimate each term on the right-hand side separately. If $J_S \neq 0$, using that H_S and J_S are constant, we get

$$\begin{aligned} |\alpha_S| \, \|\nabla \varphi_S\|_{\Omega_S} &= \frac{\left|\int_S H_S J_S^2\right|}{\left|\int_S J_S \varphi_S\right|} \|\nabla \varphi_S\|_{\Omega_S} = d\, H_S |J_S| \, \|\nabla \varphi_S\|_{\Omega_S} \\ &= d \left(\int_{\Omega_S} H_S^2 J_S^2 |\nabla \varphi_S|^2 \right)^{\frac{1}{2}} \leq C\, d \left(\int_{\Omega_S} J_S^2 \right)^{\frac{1}{2}} \\ &\leq C\, d \left(\int_S H_S J_S^2 \right)^{\frac{1}{2}} = C\, d \left\| H_S^{\frac{1}{2}} J_S \right\|_S , \end{aligned}$$

where C is a constant depending only on the minimum angle of $\mathcal{T}_h$. A similar bound is valid with φ_S replaced by φ_i. Likewise, using now that f_i is constant, we have for $f_i \neq 0$

$$|\beta_i| \leq \frac{\int_{T_i} H_i^2 f_i^2}{\int_{T_i} |f_i| \varphi_i} + \frac{|\alpha_S| \int_{T_i} |f_i| \varphi_S}{\int_{T_i} |f_i| \varphi_i} \leq C H_i^2 |f_i| + C |\alpha_S|,$$

with C depending on d and the minimum angle of $\mathcal{T}_h$. Then,

$$|\beta_i| \, \|\nabla \varphi_i\|_{\Omega_S} \leq C\, H_i^2 \; |f_i| \, \|\nabla \varphi_i\|_{T_i} + C |\alpha_S| \, \|\nabla \varphi_i\|_{T_i} \,.$$

Since

$$H_i^2 \; |f_i| \, \|\nabla \varphi_i\|_{T_i} = \left(\int_{T_i} |\nabla \varphi_i|^2 f_i^2 H_i^4 \right)^{\frac{1}{2}} \leq C \left(\int_{T_i} H_i^2 f_i^2 \right)^{\frac{1}{2}} ,$$

the desired bound (4.4) follows at once. This completes the proof. $\square$

Now we can state and prove a *global* lower bound for the error decrease.

Corollary 4.3. *Let $\mathcal{T}_h$ be a triangulation obtained from $\mathcal{T}_H$ by refining at least every element marked according to Strategy E in such a way that a node is created in the element interior. Then, we have the following global lower bound for the error reduction*

$$|\!|\!| u_h - u_H |\!|\!|_\Omega^2 \geq \frac{\theta^2}{2\, C_4\, C_1} |\!|\!| u - u_H |\!|\!|_\Omega^2 - \frac{C_5}{C_4} \operatorname{osc}(f, \mathcal{T}_H)^2.$$

Proof. By Lemma 4.2 and Step 1 of the Marking Strategy E we have

$$\begin{aligned}\theta^2\eta_H^2 &\le \sum_{S\in\hat{\mathcal{S}}_H} \eta_S^2 \le C_4 \sum_{S\in\hat{\mathcal{S}}_H} |\!|\!| u_h - u_H |\!|\!|_{\Omega_S}^2 + C_5 \sum_{S\in\hat{\mathcal{S}}_H} \|H(f-f_H)\|_{\Omega_S}^2 \\ &\le 2\,C_4\,|\!|\!| u_h - u_H |\!|\!|_{\Omega}^2 + 2\,C_5\,\|H(f-f_H)\|_{\Omega}^2 .\end{aligned}$$

Hence,

$$|\!|\!| u_h - u_H |\!|\!|_{\Omega}^2 \ge \frac{\theta^2}{2\,C_4}\eta_H^2 - \frac{C_5}{C_4}\,\|H(f-f_H)\|_{\Omega}^2 ,$$

and the assertion follows from (1.3) and Lemma 2.1. □

Lemmas 4.1, 4.2 and Corollary 4.3 have provided us with the necessary tools to prove Theorem 3.1.

Proof of Theorem 3.1. In view of Lemma 4.1 and Corollary 4.3, we have

$$\begin{aligned}|\!|\!| u - u_h |\!|\!|_{\Omega}^2 &= |\!|\!| u - u_H |\!|\!|_{\Omega}^2 - |\!|\!| u_H - u_h |\!|\!|_{\Omega}^2 \\ &\le |\!|\!| u - u_H |\!|\!|_{\Omega}^2 \left(1 - \frac{\theta^2}{2\,C_4\,C_1}\right) + \frac{C_5}{C_4}\,\mathrm{osc}(f,\mathcal{T}_H)^2 .\end{aligned}$$

Assume now that $|\!|\!| u - u_H |\!|\!|_{\Omega} > \epsilon$. Since $\mathrm{osc}(f,\mathcal{T}_H) \le \mu\epsilon$, then

$$|\!|\!| u - u_h |\!|\!|_{\Omega}^2 \le |\!|\!| u - u_H |\!|\!|_{\Omega}^2 \left(1 - \frac{\theta^2}{2\,C_4\,C_1} + \frac{C_5}{C_4}\mu^2\right) .$$

Therefore,

$$|\!|\!| u - u_h |\!|\!|_{\Omega} \le \alpha\,|\!|\!| u - u_H |\!|\!|_{\Omega}$$

where $\alpha := \left(1 - \frac{\theta^2}{2\,C_4\,C_1} + \frac{C_5}{C_4}\mu^2\right)^{1/2} < 1$ provided $\mu > 0$ is sufficiently small. □

5 Numerical Experiments

We start with a brief discussion of crucial implementation issues, and conclude with three relevant experiments which corroborate convergence of Algorithm C without mesh preadaptation, produce quasi-optimal meshes, and show a very competitive performance.

5.1 Implementation of Algorithm C

The Convergent Algorithm C is implemented within the finite element toolbox ALBERT [11, 12]. For the implementation of this algorithm, we have to change the standard adaptive solver for elliptic problems of ALBERT slightly. The following modules are added to, or replace modules of, the standard solver. They are all minor modifications.

Interior node. During the refinement of a marked element we have to ensure that an interior node is created. ALBERT uses recursive bisectioning refinement: the newest vertex refinement in 2d [10] and the algorithm of Kossaczký [9] in 3d. This leads to a sequence of *nested* grids, which is crucial in obtaining the error orthogonality of Lemma 4.1.

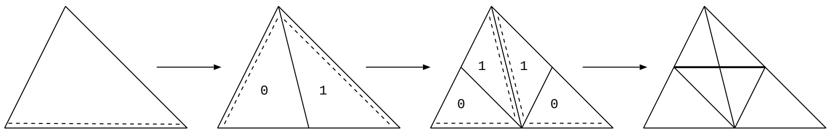

Figure 5: Refinement of triangles in 2d by newest-vertex bisection. Dashed lines indicate the refinement edges.

Creating an interior node is rather easy in 2d. First, elements are marked for two bisections and then refined. Secondly, the two grandchildren with index 1 are bisected once more. The whole refinement process is shown in Figure 5. The first refinement step may, as usual, involve surrounding elements which are not marked. This is an inevitable effect in order to preserve mesh conformity. The second refinement step is *local* in that it involves only the two grandchildren with index 1 and does not spread outside them.

In 3d it is impossible to perform the second step by dealing only with children of the original tetrahedron. The first step consists of three bisections. In order to obtain the interior node, the second step consists of marking some subtetrahedra for two or three additional bisections. This has the spreading effect of creating additional nodes in the edges of the original tetrahedron. For the implementation, we do not split the refinement into two steps, but rather mark a tetrahedron for six bisections which are performed in one step. Example 5.4 demonstrates experimentally that the additional nodes are not too many and the resulting meshes are still quasi-optimal.

Side-based error estimator. In view of (2.6), we mark sides for refinement. Usually, error indicators are stored element-wise and marking is also done element-wise. These modules are now changed in such a way that the jump residual $\|H_S^{1/2} J_S\|_S$ across a side S and the element residual $\|H\, f\|_{\Omega_S}$ of the two adjacent simplices are stored at the side S itself. The marking function thus uses side error indicators η_S and marks both adjacent elements for refinement.

According to the Marking Strategy E, we collect sides in $\hat{\mathcal{S}}_H$ with biggest side error indicators η_S until

$$\left(\sum_{S\in\hat{\mathcal{S}}_H} \eta_S^2\right)^{1/2} \geq \theta\eta_H\,.$$

In order to avoid a complicated sorting algorithm for the ordering of the error indicators, we adapt the algorithm proposed in [4]:

Algorithm 5.1 (Marking algorithm).

```
Given parameters 0 < θ, ν < 1  (θ ≈ 0.5,  ν ≈ 0.1)

η_max := max(η_S , S ∈ S_H)
sum := 0
γ := 1
while sum < θ²η_H² do
   γ := γ − ν
   for all S in S_H do
      if S is not marked
         if η_S > γ η_max
            mark both adjacent simplices for refinement
            sum := sum + η_S²
         end if
      end if
   end for
end while
```

An alternative to the side-based marking uses element-stored indicators as follows: an element is marked together with all its neighbours. This leads to a slightly larger number of marked elements but may again be viewed as a looking ahead strategy. An advantage is that only the marking strategy has to be modified.

Data oscillation. The last module we supply is a function which marks elements due to data oscillation, i.e., an implementation of Marking Strategy D. For each simplex T, we compute the mean value f_T of f on T and store the value $\|H(f - f_T)\|_T$. Given $\hat{\theta}$ and $\hat{\mathcal{T}}_H$, the set of marked elements by Algorithm 5.1, we enlarge $\hat{\mathcal{T}}_H$ in such a way that

$$\operatorname{osc}(f, \hat{\mathcal{T}}_H) \geq \hat{\theta} \operatorname{osc}(f, \mathcal{T}_H)$$

holds. If this inequality is satisfied by $\hat{\mathcal{T}}_H$, we are done. Otherwise, we use a slight modification of Algorithm 5.1 to mark additional elements. This is now done element-wise using the oscillation $\|H(f - f_T)\|_T$ of f as an indicator.

5.2 Example: Crack Problem

We consider the domain $\Omega = \{|x| + |y| < 1\} \backslash \{0 \leq x \leq 1, y = 0\}$ with a crack and the function u in polar coordinates

$$u(r, \theta) = r^{\frac{1}{2}} \sin \tfrac{\theta}{2} - \tfrac{1}{4} r^2 .$$

We solve (1.2) with $A = I$ and $f = 1$, and a non-vanishing Dirichlet boundary condition on $\partial\Omega$.

We compare the Guaranteed Error Reduction Strategy (GERS) of Dörfler [4] with our Convergent Strategy (CONV). Using GERS, all marked triangles are only bisected twice; the interior node is not created. Since $f \neq 0$ GERS requires an initial mesh refinement to satisfy the mesh fineness condition; since $f \equiv 1$ this initial mesh refinement is a global refinement. Strategy CONV does not need these preadaptation step; CONV thus starts from a very coarse mesh.

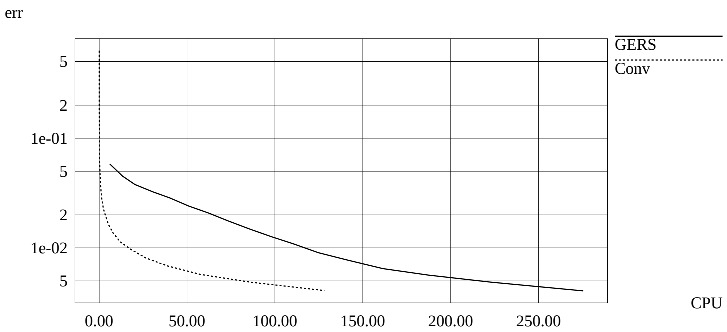

Figure 6: Comparison of CPU time for GERS and CONV.

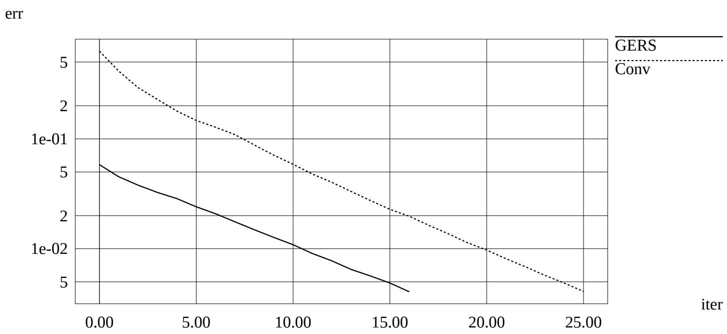

Figure 7: Comparison of reduction rate α^k for GERS, CONV.

Figure 6 displays a superior performance of CONV in terms of computing time (CPU) due to the coarser initial grid for CONV. From Figure 7 we realize that the reduction rate α^k as a function of the iteration number k is comparable for GERS and CONV, the latter being above because CONV starts from a coarser mesh and thus requires more iterations for the same accuracy. Combining both figures we learn that CONV needs more adaptive iterations to reduce the error below the tolerance 0.05 than GERS but only half the CPU time.

Quite revealing is Figure 8. It shows the asymptotic relation $|\!|\!| u - u_k |\!|\!|_\Omega = C$ $\mathrm{DOFs}(k)^{-1/2}$ typical of quasi-optimal meshes in 2d and thus of quasi-optimal numerical complexity. In the log-log plot the optimal decay of $|\!|\!| u - u_k |\!|\!|_\Omega$ is a straight line with slope $-1/2$. This line is also plotted in Figure 8.

Figure 9 displays the grid of CONV for iteration 18, and three zooms at the origin. The rather strong grading of the quasi-optimal partition is quite

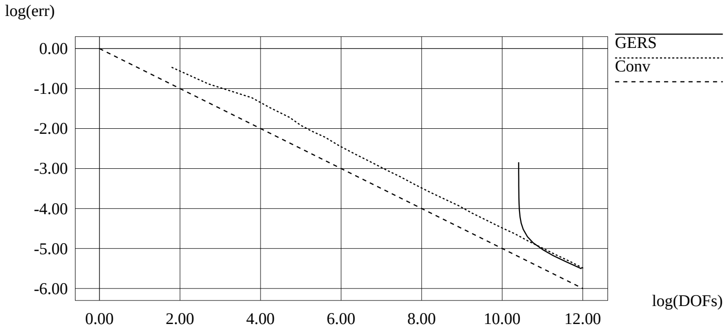

Figure 8: Quasi-optimality of GERS and CONV. The optimal decay is indicated by the dashed line with slope $-1/2$.

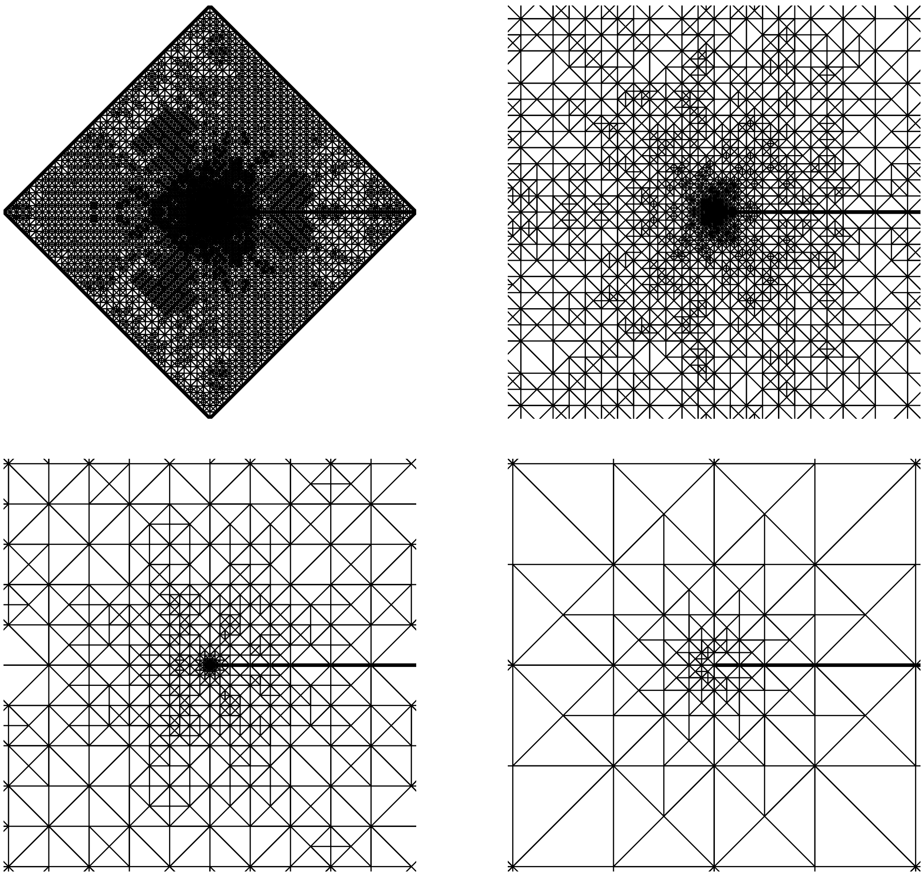

Figure 9: Adaptive grids for iteration 18 of the CONV strategy: full grid (upper left), zoom to $(-5\,10^{-2}, 5\,10^{-2})^2$ (upper right), zoom to $(-2.5\,10^{-3}, 2.5\,10^{-3})^2$ (lower left), and zoom to $(-1.25\,10^{-4}, 1.25\,10^{-4})^2$ (lower right).

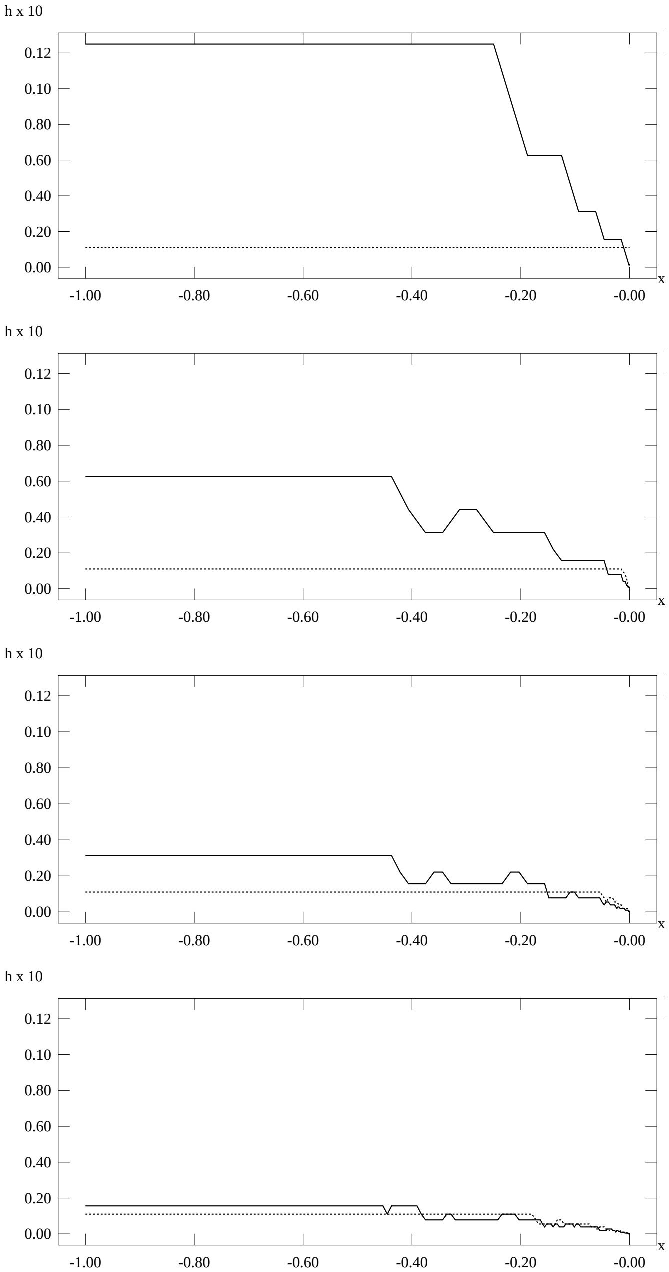

Figure 10: Comparison of local meshsizes h on the line $y = 0$ for GERS (dotted line) and CONV (solid line) on meshes with approximately same errors $\|u - u_k\|_\Omega$.

apparent.

In order to compare the different local meshsizes for GERS and CONV due to the preadaptation of GERS, we plot the meshsizes along the segment $\{-1 < x < 0, y = 0\}$ in Figure 10. We choose the meshes in such a way that the error on the respective meshes is approximately the same for GERS and CONV. The pictures correspond (from top to bottom) to the meshes in iteration 0, 4, 8, and 12 of GERS with errors $\|u - u_k\|_\Omega \approx$ 5.8-e02, 2.8-e02, 1.4-e02, and 7.7e-03 and iterations 10, 14, 18, and 22 of CONV with errors 5.8-e02, 2.7-e02, 1.3-e02, and 6.8e-03. We realize the strong effect of mesh preadaptation needed by GERS: in contrast to CONV, GERS has to reduce the meshsize solely near the origin. This corroborates our claim that mesh preadaptation is unnecessary for constant right-hand sides f.

Finally, we compare CONV with the Maximum Strategy (MS), which is not known to converge but is the strategy of choice among practitioners. Figure 11 depicts a similar performance of both CONV and MS in terms of DOFs.

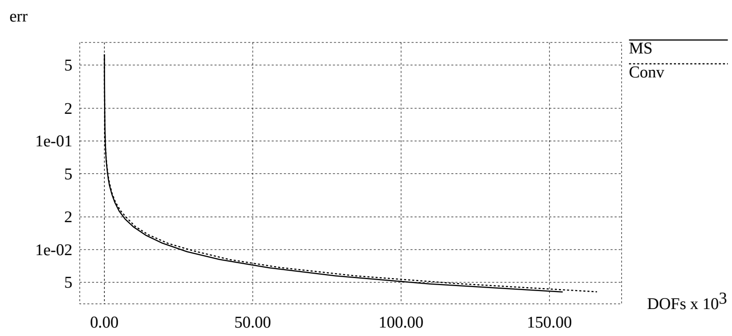

Figure 11: Comparison of CONV and MS.

5.3 Example: Discontinuous Coefficients

We invoke the formulas derived by Kellogg [8] to construct an exact solution of an elliptic problem with piecewise constant coefficients and vanishing right-hand side f; data oscillation is thus immaterial. We now write these formulas in the particular case $\Omega = (-1,1)^2$, $A = a_1 I$ in the first and third quadrants, and $A = a_2 I$ in the second and fourth quadrants. An exact weak solution u of (1.2) for $f \equiv 0$ is given in polar coordinates by $u(r,\theta) = r^\gamma \mu(\theta)$, where

$$\mu(\theta) = \begin{cases} \cos((\pi/2 - \sigma)\gamma) \cdot \cos((\theta - \pi/2 + \rho)\gamma) & \text{if } 0 \le \theta \le \pi/2 \\ \cos(\rho\gamma) \cdot \cos((\theta - \pi + \sigma)\gamma) & \text{if } \pi/2 \le \theta \le \pi \\ \cos(\sigma\gamma) \cdot \cos((\theta - \pi - \rho)\gamma) & \text{if } \pi \le \theta < 3\pi/2 \\ \cos((\pi/2 - \rho)\gamma) \cdot \cos((\theta - 3\pi/2 - \sigma)\gamma) & \text{if } 3\pi/2 \le \theta \le 2\pi \end{cases}$$

and the numbers γ, ρ, σ satisfy the nonlinear relations

$$\begin{cases} R := a_1/a_2 = -\tan((\pi/2-\sigma)\gamma)\cdot\cot(\rho\gamma) \\ 1/R = -\tan(\rho\gamma)\cdot\cot(\sigma\gamma) \\ R = -\tan(\sigma\gamma)\cdot\cot((\pi/2-\rho)\gamma) \\ 0<\gamma<2 \\ \max\{0,\pi\gamma-\pi\} < 2\gamma\rho < \min\{\pi\gamma,\pi\} \\ \max\{0,\pi-\pi\gamma\} < -2\gamma\sigma < \min\{\pi, 2\pi-\pi\gamma\}. \end{cases} \tag{5.1}$$

Since we want to test the algorithm CONV in some worst case scenario, we choose $\gamma = 0.1$, which produces a very singular solution u that is barely in H^1. We then solve (5.1) for R, ρ and σ using Newton's method to obtain

$$R = a_1/a_2 \cong 161.4476387975881, \qquad \rho = \pi/4, \qquad \sigma \cong -14.92256510455152,$$

and finally choose $a_1 = R$ and $a_2 = 1$. A smaller γ would lead to a larger ratio R, but in principle γ may be as close to 0 as desired.

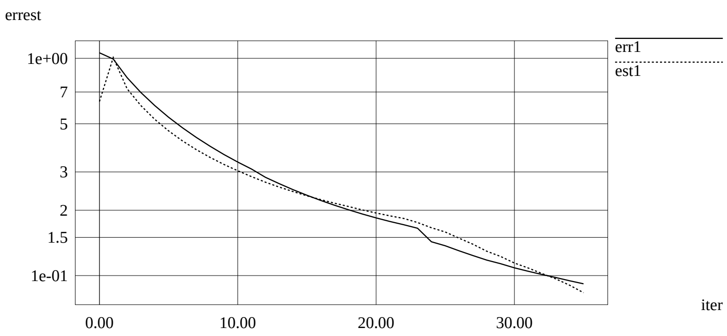

Figure 12: Error reduction: estimate and true error.

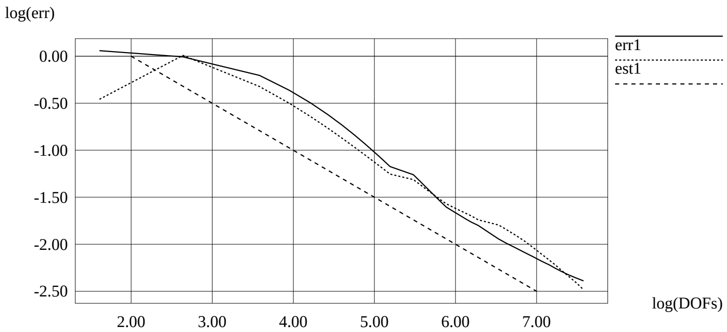

Figure 13: Quasi-optimality of CONV: estimate and true error. The optimal decay is indicated by the dashed line with slope $-1/2$.

In Figures 12-13 we see the same behavior of the true error $\|u - u_k\|_\Omega$ and the estimator η_k. Figure 13 demonstrates that the grids and associated numerical complexity are quasi-optimal: $\|u - u_k\|_\Omega = C \text{ DOFs}(k)^{-1/2}$ is valid asymptotically (the performance of an optimal method is again indicated by the additional straight line)!

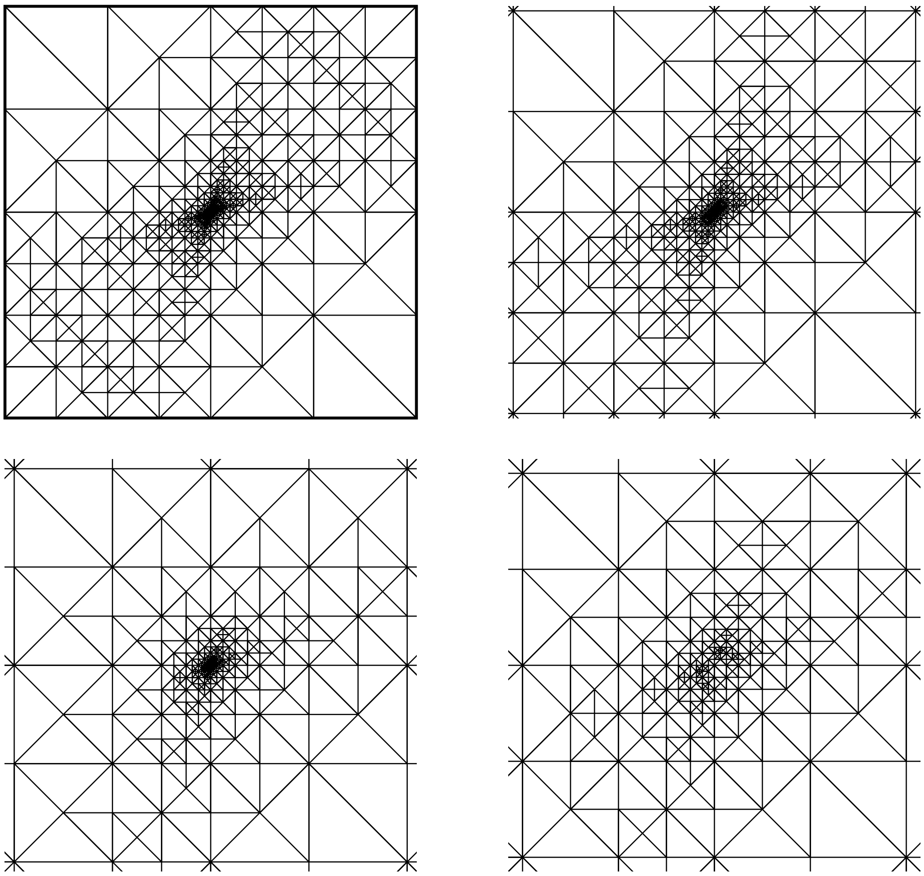

Figure 14: Final grid: full grid with < 2000 nodes (upper left), zoom to $(-10^{-3}, 10^{-3})^2$ (upper right), zoom to $(-10^{-6}, 10^{-6})^2$ (lower left), and zoom to $(-10^{-9}, 10^{-9})^2$ (lower right).

For this problem the grid is highly graded at the origin. It is worth to realize the strength of the singularity at hand in Figure 14. We see a mesh with < 2000 nodes and three zooms at the origin, each obtained with a magnifying factor 10^3, and yet exhibiting a rather strong grading. This is also reflected in Figure 15, which depicts the graph of the discrete solution over the underlying mesh: the solution is flatter in the quadrants with $a \approx 161$ although the grid is finer, which accounts for the presence of a in the energy norm. This picture was created using the graphics package GRAPE [7]. This example is much more

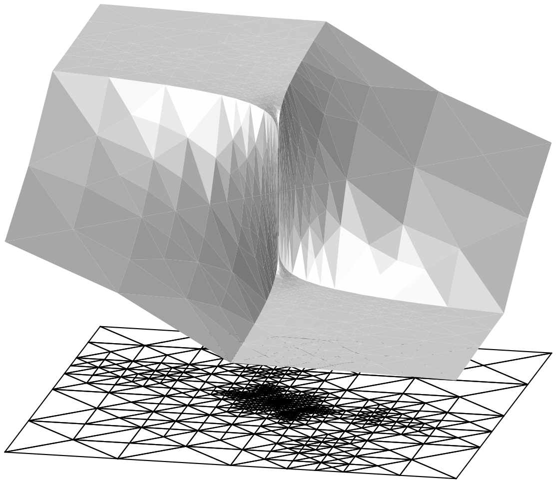

Figure 15: Graph of the discrete solution and underlying grid.

singular than Example 5.2 and seems to be new in the finite element literature.

5.4 Example: Variable Source

In Examples 5.2 and 5.3 the source term is constant. It is our purpose now to examine the effect of data oscillation (1.3). To this end, we consider the domain $\Omega = (-1,1)^d$ with $d = 2,3$, and the exact solution

$$u(x) = \mathrm{e}^{-10\,|x|^2}$$

of (1.2) with $A = I$ and non-constant $f = -\Delta u$. Such an f exhibits a relatively large variation in Ω, and within elements, which forces Algorithm C to refine additional elements due to data oscillation, not yet marked for refinement by Strategy E (Step 6 of Algorithm C). This is reported in Table 1 for 2d (left table) and 3d (right table). We see that the number of additional elements due to large data oscillation is rather small relative to those due to large error indicators, but it is *not* zero. On the one hand, this confirms that control of data oscillation cannot be omitted in a convergent algorithm. On the other hand, this explains why data oscillation seems to play a minor role for (piecewise) smooth data f, and hints at the underlying reasons why most adaptive strategies, although neglecting data oscillation, converge in practice.

As mentioned in Section 5.1, we produce in 3d the interior node by bisecting a marked tetrahedron six times. This corresponds in 2d to four bisections of a marked triangle, which is used here instead of the procedure of Figure 5. Although this produces more DOFs than needed, Figures 16 and 17 demonstrate that the resulting meshes are still quasi-optimal for both 2d and 3d. For comparison with an optimal mesh, dashed lines with slope $-1/d$ are plotted in Figure 16) ($d = 2$) and Figure 17 ($d = 3$); note that these lines have the same slope due to different scaling of the y axis.

iter.	error est.	oscillation
0	8	0
1	16	16
2	56	8
3	80	0
4	96	8
5	112	24
6	344	0
7	432	0
8	608	0
9	768	16
10	2192	0
11	2296	24
12	3816	24

iter.	error est.	oscillation
0	48	0
1	48	48
2	576	0
3	5040	0
4	5136	720
5	30144	0

Table 1: Number of elements marked per iteration in 2d (left) and 3d (right) due to error estimator and additionally to data oscillation.

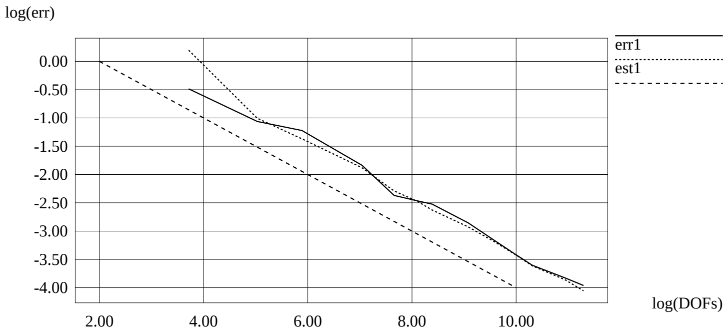

Figure 16: Quasi-optimality of CONV: estimate and true error in 2d. The optimal decay is indicated by the line with slope $-1/2$.

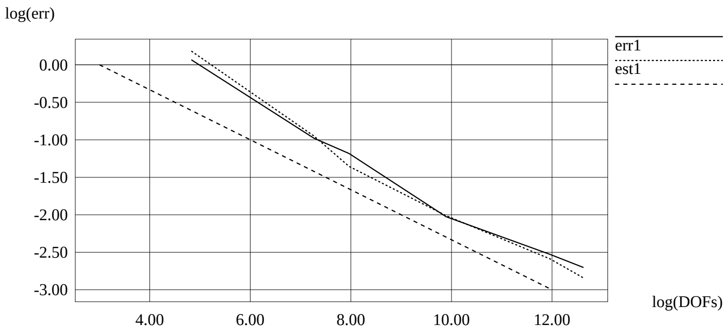

Figure 17: Quasi-optimality of CONV: estimate and true error in 3d. The optimal decay is indicated by the line with slope $-1/3$.

Finally, in Figure 18 we cut $(0,1)^3$ out of the domain $(-1,1)^3$ and show the adaptive grid of the 3d simulation on the boundary of the resulting domain. In the left picture we show the full grid of the 2nd iteration and in the right one a zoom into the grid of the 4th iteration. For this picture we also used the graphics package GRAPE.

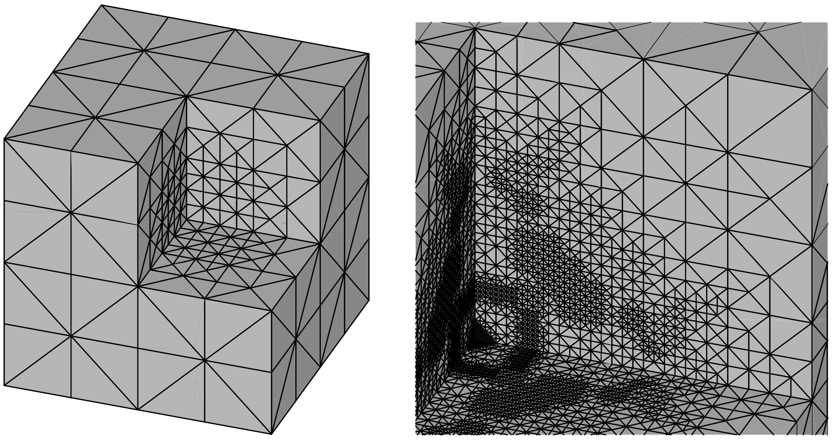

Figure 18: Adaptive grids of the 3d simulation on $\partial((-1,1)^3 \backslash (0,1)^3)$: full grid of the 2nd iteration (left), zoom into the grid of the 4th iteration.

References

[1] I. Babuška and A. Miller, *A feedback finite element method with a posteriori error estimations: Part I. The finite element method and some basic properties of the a posteriori error estimator*, Computer Meth. Appl. Mech. Eng., 61 (1987), 1-40.

[2] I. Babuška and M. Vogelius, *Feedback and adaptive finite element solution of one-dimensional boundary value problems*, Numer. Math., 44 (1984), 75-102.

[3] A. Cohen, W. Dahmen, R. DeVore, *Adaptive wavelet methods for elliptic operator equations — convergence rates*, preprint.

[4] W. Dörfler, *A convergent adaptive algorithm for Poisson's equation*, SIAM J. Numer. Anal., 33 (1996), 1106-1124

[5] W. Dörfler, *A robust adaptive strategy for the nonlinear Poisson equation*, Computing, 55 (1995), 289-304.

[6] W. Dörfler, O. Wilderotter, *An adaptive finite element method for a linear elliptic equation with variable coefficients*, Preprint 1-99, Univ. Freiburg.

[7] GRAPE — *GRAphics Programming Environment*, Manual, Version 5.0 (1995), SFB 256, Univ. Bonn.

[8] R.B. Kellogg, *On the Poisson equation with intersecting interfaces*, Applicable Analysis, 4 (1975), 101-129.

[9] I. Kossaczký, *A recursive approach to local mesh refinement in two and three dimensions*, J. Comput. Appl. Math., 55 (1994), 275-288.

[10] W. Mitchell, *A comparison of adaptive refinement techniques for elliptic problems*, ACM Trans. Math. Softw., 15 (1989), 210–227.

[11] A. Schmidt and K.G. Siebert, *ALBERT: An adaptive hierarchical finite element toolbox*, Documentation (in preparation).

[12] A. Schmidt and K.G. Siebert, *Concepts of the finite element toolbox ALBERT*, Preprint 17/98 Freiburg, to appear in Notes on Numerical Fluid Mechanics.

[13] R. Verfürth, *A Review of A Posteriori Error Estimation and Adaptive Mesh-Refinement Techniques*, Wiley-Teubner, 1995.

Pedro Morin
Department of Mathematics, University of Maryland, College Park, MD 20742, USA.
Permanent Address: Departamento de Matemática, Facultad de Ingeniería Química, Universidad Nacional del Litoral, Argentina.
Partially supported by Programa FOMEC de la Universidad Nacional del Litoral, CONICET of Argentina, and NSF Grants DMS-9623394 and DMS-9971450.
Email: `pmorin@math.umd.edu`.
`http://www.math.umd.edu/~pmorin`.

Ricardo H. Nochetto
Department of Mathematics and Institute for Physical Science and Technology, University of Maryland, College Park, MD 20742, USA.
Partially supported by NSF Grants DMS-9623394 and DMS-9971450.
Email: `rhn@math.umd.edu`.
`http://www.math.umd.edu/~rhn`.

Kunibert G. Siebert
Institut für Angewandte Mathematik, Hermann-Herder-Str. 10, 79104 Freiburg, Germany.
Email: `kunibert@mathematik.uni-freiburg.de`.
`http://www.mathematik.uni-freiburg.de/IAM/homepages/kunibert`
This work was developed while this author was visiting the University of Maryland.